

Blockage of Anthrax PA₆₃ Pore by a Multicharged High-Affinity Toxin Inhibitor

Ekaterina M. Nestorovich,^{†*} Vladimir A. Karginov,[§] Alexander M. Berezhkovskii,[‡] and Sergey M. Bezrukov[†]

[†]Laboratory of Physical and Structural Biology, Program in Physical Biology, Eunice Kennedy Shriver National Institute of Child Health and Human Development, and [‡]Mathematical and Statistical Computing Laboratory, Division of Computational Bioscience, Center for Information Technology, National Institutes of Health, Bethesda, Maryland; and [§]Innovative Biologics, Herndon, Virginia

ABSTRACT Single channels of *Bacillus anthracis* protective antigen, PA₆₃, were reconstituted into planar lipid membranes and their inhibition by cationic aminopropylthio- β -cyclodextrin, AmPr β CD, was studied. The design of the highly efficient inhibitor, the sevenfold symmetrical cyclodextrin molecule chemically modified to add seven positive charges, was guided by the symmetry and predominantly negative charge of the PA₆₃ pore. The protective action of this compound has been demonstrated earlier at both single-molecule and whole-organism levels. In this study, using noise analysis, statistics of time-resolved single-channel closure events, and multichannel measurements, we find that AmPr β CD action is bimodal. The inhibitor, when added to the *cis* side of the membrane, blocks the channel reversibly. At high salt concentrations, the AmPr β CD blockage of the channel is well described as a two-state Markov process, in which both the on- and off-rates are functions of the salt concentration, whereas the applied voltage affects only the off-rate. At salt concentrations smaller than 1.5 M, the second mode of AmPr β CD action on the channel is discovered: addition of the inhibitor enhances voltage gating, making the closed states of the channel more favorable. The effect depends on the lipid composition of the membrane.

INTRODUCTION

Recent years have brought significant progress in understanding anthrax intoxication that involves a channel-facilitated protein translocation system (1,2). Anthrax toxin, as a member of the bacterial AB-type exotoxin family, consists of three proteins that self-assemble at the surface of the cell. One of the proteins, protective antigen of 83 kDa (PA₈₃), binds to specific cellular receptors and is cleaved by a furin-like protease of the host cell into two fragments, PA₂₀ and PA₆₃. The latter self-assembles to form a ring-shaped heptameric prepore (3,4) that can simultaneously bind several molecules of two other proteins: lethal factor and/or edema factor. The complex is then endocytosed and acidic conditions inside the endosome induce conversion of the prepore to a pore (1), which is thought to be used as a tunnel for transporting lethal factor and edema factor into the cytosol (5,6).

One of the novel approaches (7–9) to inactivation of bacterial pore-forming toxins is based on the idea (10) of blocking oligomeric channels by low-molecular-weight charged compounds that have the same symmetry as the target pores (Fig. 1). In particular, it was shown that a number of sevenfold symmetrical positively charged derivatives of β -cyclodextrin (β -CD) blocked the pore formed by *Bacillus anthracis* protective antigen (PA) and were highly efficient protective agents against anthrax lethal and edema toxins. This was demonstrated both in cell-based assays and in animal tests (7–9).

The ability of small molecules carrying one or two positive charges to block ion current through the anthrax channel was shown earlier (11–14). Recently it was extended to

a library of 35 quaternary ammonium and phosphonium ions to find the equilibrium dissociation constant, K_D , with values as low as 35 nM ((15) and its supporting materials). Structure-inspired design of the blocker guided by the symmetry and predominantly negative charge of the PA₆₃ pore (3,16–18) allowed us to bring the K_D values to as low as 70 pM in 0.1 M KCl (8). One particular derivative, per-6-(3-aminopropylthio)- β -cyclodextrin (AmPr β CD), proved to be among the most efficient pore blockers. It was shown (7) that parameters of the blockage strongly depend on the applied transmembrane voltage and bathing electrolyte concentration, suggesting the importance of electrostatic interactions in AmPr β CD binding to the anthrax pore.

Here we extend this study to examine important features of AmPr β CD interactions with the PA₆₃ pore. We start with a description of the pore conformational dynamics, and show that its voltage gating is lipid-dependent. Then, we quantify the effect of AmPr β CD concentration, applied voltage, and KCl concentration on the kinetic parameters of the binding using single-channel current recording statistics as well as noise power spectrum analysis. We demonstrate that the channel inhibition by AmPr β CD is bimodal: at low salt concentrations, in addition to a simple two-state Markovian blockage, the inhibitor acts on the channel gating by favoring channel closed states in a lipid-dependent manner.

MATERIALS AND METHODS

Reagents

PA₆₃ was prepared from PA₈₃ by limited trypsin digestion or directly purchased from List Biological Laboratories (Campbell, CA) in the purified form. For a series of test-experiments, we also used PA₆₃ kindly provided by

Submitted January 13, 2010, and accepted for publication March 31, 2010.

*Correspondence: nestoroe@mail.nih.gov

Editor: Edward H. Egelman.

© 2010 by the Biophysical Society
0006-3495/10/07/0134/10 \$2.00

doi: 10.1016/j.bpj.2010.03.070

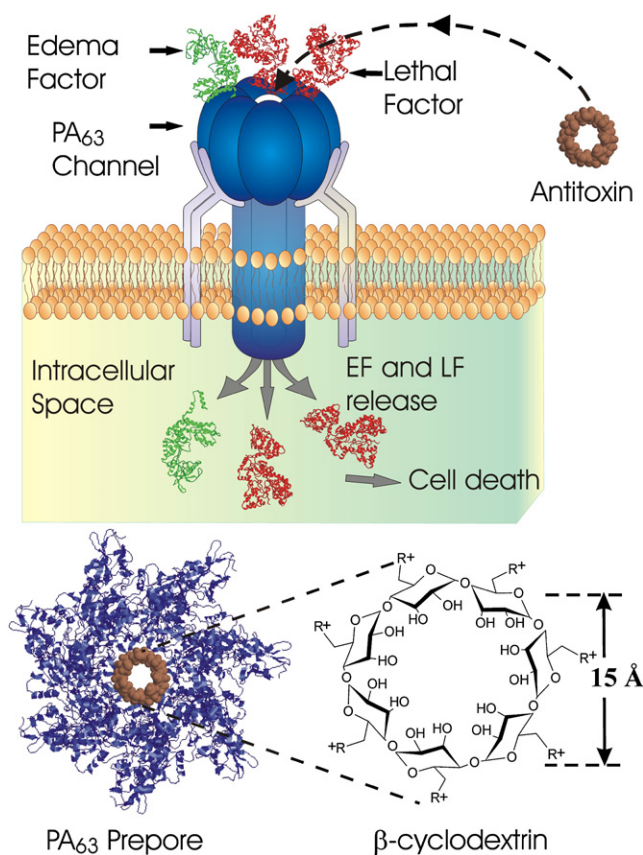


FIGURE 1 Blocking anthrax on a single-channel level. (*Top*) A heptameric mushroomlike channel of PA₆₃ produced by *Bacillus anthracis* believed to be a translocation pathway for lethal and edema factor (LF and EF) inside the cell under attack. The idea is to design complementary heptameric low-molecular weight compounds—cationic cyclodextrins (*bottom*) that enter the pore and block it as molecular plugs. PA₆₃ prepore, LF, and EF crystal structures reported in the literature (34–36) were used for the figure preparation. The cartoon is a simplified illustration of the LF and EF penetration into the mammalian cell. In reality, the process is much more complex (1).

Dr. S. Leppla (National Institutes of Health, National Institute of Allergy and Infectious Diseases). AmPr β CD was custom-synthesized at Pinnacle Pharmaceuticals (Charlottesville, VA) with the details of the synthesis given earlier (8).

The following chemical reagents were used: KCl, KOH, and HCl; MES; purum hexadecane (Fluka, Buchs, Switzerland); diphytanoyl phosphatidylcholine (PC), diphytanoyl phosphatidylserine (PS) (Avanti Polar Lipids, Alabaster, AL); pentane (Burdick and Jackson, Muskegon, MI), and agarose (Bethesda Research Laboratory, Gaithersburg, MD). Doubly distilled and deionized water was used to prepare solutions. All solutions were purified by filtration through a 0.45- μ m filter.

Channel reconstitution

To form solvent-free planar lipid bilayers with the lipid monolayer opposition technique (19), we used a 0.5% solution of PC or PS in pentane. Bilayer lipid membranes were formed on a 60- μ m (for single-channel measurements) or 150- μ m (for multichannel measurements) diameter aperture in the 15- μ m-thick Teflon film that separated two compartments as described elsewhere (20). Single channels were formed by adding 0.5–1 μ L of 20 μ g mL⁻¹ stock solution of PA₆₃ to 1.5 mL aqueous phase in the *cis*

half of the chamber. For multichannel experiments, we applied ~1–2 μ L of 0.2 mg mL⁻¹ stock PA₆₃. Under this protocol, PA₆₃ channel insertion was always directional. The electrical potential difference across the bilayer lipid membrane was applied with a pair of Ag-AgCl electrodes in 2 M KCl, 1.5% agarose bridges. The applied potential is defined as positive if it is higher at the side of PA₆₃ addition (*cis* side).

Low-binding polymer technology products were used for cyclodextrin storage, dilution, and sampling (Sorenson BioScience, Salt Lake City, UT). Conductance measurements were performed using an Axopatch 200B amplifier (Axon Instruments, Foster City, CA) in the voltage-clamp mode. Signals were filtered by a low-pass eight-pole Butterworth filter (Model 9002; Frequency Devices, Haverhill, MA) at 15 Hz for multichannel and 15 kHz for single-channel experiments and sampled with frequencies of 50 Hz and 50 kHz, respectively. For the presentations purposes, current recordings were additionally filtered at 100 ms or 1 ms for the traces in Fig. 2 A, 100 ms or 5 ms in Fig. 2 B, 10 ms in Fig. 3 A, 50 ms in Fig. 5 A, 500 ms in Fig. 7 D, and 1 s in Fig. 2 C and Fig. 7 A.

RESULTS AND DISCUSSION

Channel in the absence of inhibitor

Two types of PA₆₃ insertions

To characterize and quantify the AmPr β CD-pore interactions, we first studied the channel dynamics in the absence of the blocker. PA₆₃ forms a large cation-selective channel that irreversibly inserts into the bilayer membranes. Fig. 2 A illustrates ionic current through the PA₆₃ channel recorded under applied voltage of +30 and -30 mV at 100-ms and 1-ms time resolution in PC bilayers bathed by 1 M KCl, pH 6.6. Channel properties obtained from our recordings are similar to those described earlier (5,11–14,21). PA₆₃ conductance in 1 M KCl is sublinear in salt concentration between 0.1 and 2.5 M KCl, changing from ~80 pS to ~320 pS, correspondingly, at 20 mV of applied voltage. The channel exhibits spontaneous reversible stepwise transitions to a substate of higher conductance (11). The relative probabilities of the substate varied significantly from channel to channel.

We also observed the formation of PA₆₃ channels directly in the substate of higher conductance. In Fig. 2 B, we compare two events of PA₆₃ insertions: type I, when the channel appears in the lower-conducting state (recordings at the *top*), and type II, corresponding to the higher-conducting state insertion (recordings at the *bottom*). At the type I insertion, the channel, from time to time, reversibly switches to the higher-conducting state (*top*), whereas at the type II insertion (*bottom*), the current through the channel is more stable. These observations might be related to the recently discussed possibility of two different oligomerization states of the channel (22). Based on our data on conductances of single PA₆₃ channels in 1 M KCl at pH 6.6, we estimate the ratio of type I to type II insertions to be close to 3:2 (namely 44 type I versus 31 type II insertions). Both increasing salt concentration and lowering solution pH slightly shifted this ratio in favor of type II insertions. We recorded 12 type I versus 13 type II insertions in 1.5–2.5 M KCl at pH 6.6 and 35 type I versus 130 type II in 1 M KCl at pH 5.5. In lower KCl concentrations and especially in DPhPS membranes,

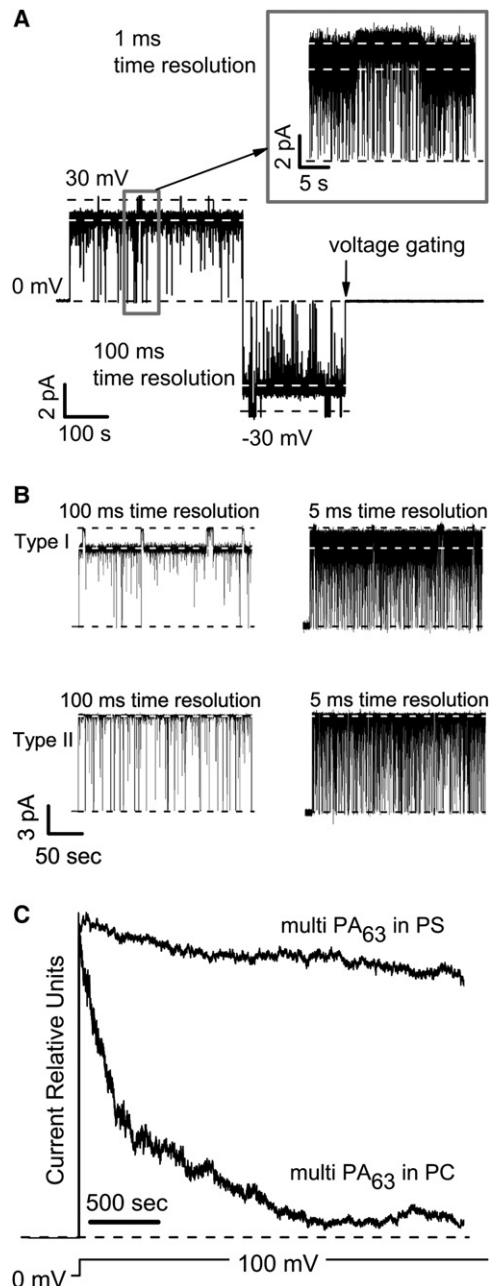


FIGURE 2 Two types of PA_{63} insertion and gating. (A) Typical track of ion current through a single PA_{63} pore in type I insertion recorded at 30 and -30 mV. The dashed lines show zero current level and two distinct conductance levels. (Inset) Part of the main recording at higher time resolution. Time averaging used for plots was 100 ms (main recording) and 1 ms (inset). (B) Currents through single channels for insertions of type I (two traces at the top) and type II (two traces at the bottom) at 50-mV applied voltage. Recordings on the left (top and bottom) are shown at 100-ms time resolution, recordings on the right at 5-ms resolution. The membranes were formed from PC. The membrane bathing solutions contained 1 M KCl and 5 mM MES at pH 6.6. (C) Multichannel recordings show clear difference in PA_{63} voltage gating in neutral PC and negatively charged PS bilayer membranes. Application of 100 mV closes channels in PC bilayers much more efficiently than in PS bilayers. Recordings were taken in 0.1 M KCl solution at pH 6.6. (Dashed line) Level of zero current. Time averaging used for plots was 1 s.

we observed significant shift of the ratio in favor of type I insertion. We recorded 31 type I insertions versus 13 type II insertions in 0.3–0.75 M KCl at pH 6.6. In DPhPS lipid membranes, we recorded 33 type I versus 3 type II insertions in 1 M KCl at pH 6.6. Note that at lower KCl concentrations and at pH 5.5, small conductance steps corresponding to reversible switching to the higher channel conductance at type I insertion were not clearly visible. In DPhPS membranes the steps were frequent and close to 30% of the total channel conductance (data not shown).

Slow voltage-dependent and fast voltage-independent gating

In addition to the switching between the two well-resolved high-conducting states of the channel described above, we also detected two types of complex non-Markovian channel gating. The first type is promoted by the applied voltage. It brings the channel to nonconductive states (see, for example, Fig. 2 A, -30 mV recording). This voltage gating is more pronounced at negative voltages (5,11,12,14,23), a circumstance that significantly limited our ability to collect reliable statistics at negative biases. After the closure at negative voltages, the channel tended to stay at a low-conductive state for minutes and in a number of cases, reopening was not observed on a timescale of several hours even after the applied voltage was reduced to zero. However, second-long pulses of voltages as high as 250 mV often made channel reopening possible. This behavior resembles the voltage-induced closure observed in many known β -barrel proteins reconstituted in lipid bilayers (24). Recently, the voltage-dependent gating of cysteine-substituted PA_{63} channels was reported to be abolished by a reaction with a methanethiosulfonate reagent that catalyzes the formation of intersubunit disulfide bonds (23). We found that PA_{63} voltage gating is lipid-dependent. Fig. 2 C shows that channels are much less sensitive to the applied voltage if reconstituted in PS membranes compared with PC membranes.

The second type of gating is illustrated by the higher-resolution current recording shown in Fig. 2. It is seen as voltage-independent fast flickering (11) between the open and completely closed states. Fast flickering of PA_{63} is an intrinsic property of this channel occurring at both type I and type II insertions (Fig. 2 B). The current noise power spectra of the PA_{63} channel at both types of insertions contain a $1/f$ -like component that is proportional to the applied voltage squared (see below). This finding agrees with the multichannel experiments (14) where $1/f$ noise for the PA_{63} channels has also been reported.

In contrast to β -barrels voltage gating, which is sometimes believed to be an artifact of bilayer lipid membrane experiments, voltage-independent PA_{63} fast flickering between the conductive and nonconductive states may be due to the pore structural flexibility. If true, this phenomenon deserves to be studied in more detail in light of the key role of the channel in lethal factor and edema factor translocation into the cell (6,15).

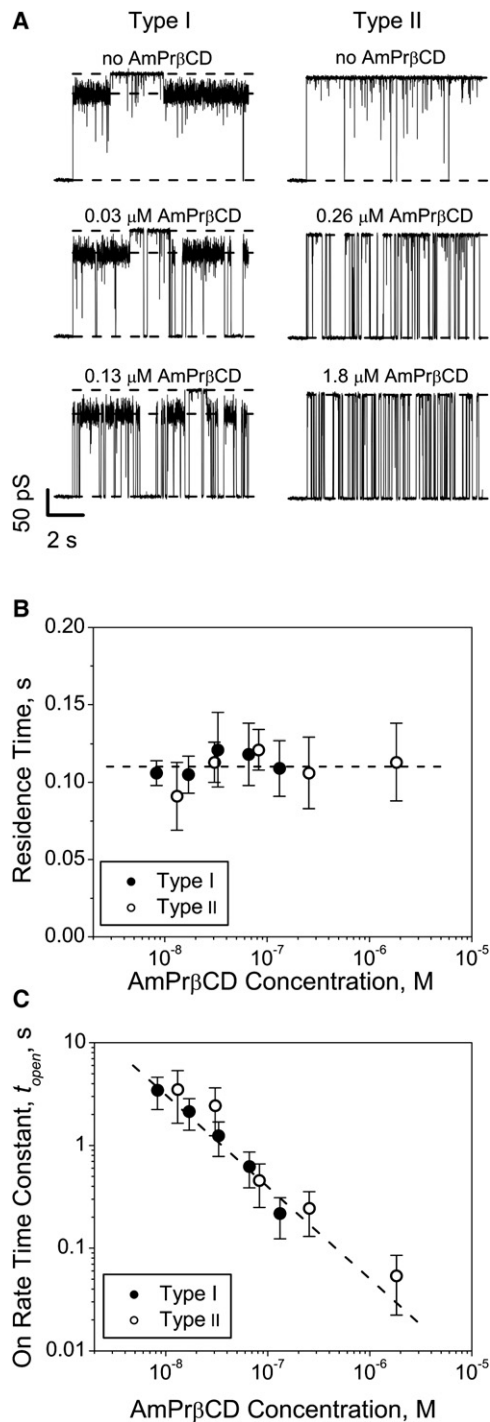


FIGURE 3 AmPr β CD blocks PA₆₃ pore at type I and type II insertions. (A) AmPr β CD addition to the *cis* side of the membrane modulates ion current through a single channel both for type I (left) and type II (right) insertions. In the absence of AmPr β CD (top), fast flickering between open and closed states was mainly removed by averaging over a time interval of 10 ms. In the presence of AmPr β CD, the channel gets spontaneously blocked (middle and bottom). (Dashed line) Zero current levels and two different conductance levels. (B) The average time of the AmPr β CD-induced blockages does not depend on the blocker concentration. (Dashed line) Averaged residence time equal to 110 ms. The data were obtained for two insertion types: type I (solid circles) and type II (open circles).

AmPr β CD-pore interactions

Two types of PA₆₃ insertions

We first compared channel blockage by AmPr β CD at the two types of insertion with the goal to check whether the channels at both insertions are equally susceptible to the blocker. The current tracks recorded at different AmPr β CD concentrations for the type I (left) and type II (right) insertions are shown in Fig. 3 A for PC bilayers bathed by 1 M KCl solutions at pH 6.6. In the absence of AmPr β CD (top), the ion flow through both channels is rather noisy due to the conformational dynamics of the pore discussed above. Fast flickering between open and closed states is mainly removed here by averaging over a time interval of 10 ms. In the presence of AmPr β CD in the *cis* side of the chamber, the channel gets spontaneously blocked with the frequency of blockages depending on AmPr β CD concentration (middle and bottom). Within the accuracy of our measurements, these blockages are complete and are described by the same on- and off-rates (Fig. 3, B and C).

The conductance fluctuations induced by AmPr β CD in the parts of the recordings with excluded voltage-dependent gating can be described as a two-state Markov process. This is manifested by an approximately single-exponential distribution for the duration of AmPr β CD blockages and by the Lorentzian shape of power spectral density of the AmPr β CD-induced fluctuations (Fig. 4). Both direct single-exponential fitting of the residence time histograms and current noise analysis were used to measure the average blockage time of the channel, t_{res} , shown in Fig. 3 B. The main difficulty with the direct residence time fitting was to separate the AmPr β CD-induced blockages from the fast flickering. The equal amplitudes of the current fluctuations for these two processes complicated the problem. However, substantially different distributions of the blockage times made this separation possible.

Fig. 4 A represents two typical histograms obtained by collecting the times of fast-flickering gating events in AmPr β CD-free solutions (solid histogram) and the times of these gating events plus AmPr β CD-induced blockages recorded in blocker containing solutions (shaded bars). Fig. 4 B shows the histogram difference, with the high-frequency gating events excluded. We first adjusted the amplitude of the gating histogram using short time bins (≤ 0.3 ms) to the histogram of gating events plus blockages shown on Fig. 4 A and then subtracted the former from the latter.

Note that Fig. 4 represents one of the most challenging examples of data analysis where fast-flickering gating events and AmPr β CD-induced blockages overlap. At lower salt

(C) The time between blockages is inversely proportional to AmPr β CD bulk concentration for both type I (solid circles) and type II (open circles) insertions. (Dashed line) Linear fit through all data. All the data were obtained from experiments with PC membranes performed under 50-mV applied voltage in 1 M KCl and 5 mM MES at pH 6.6.

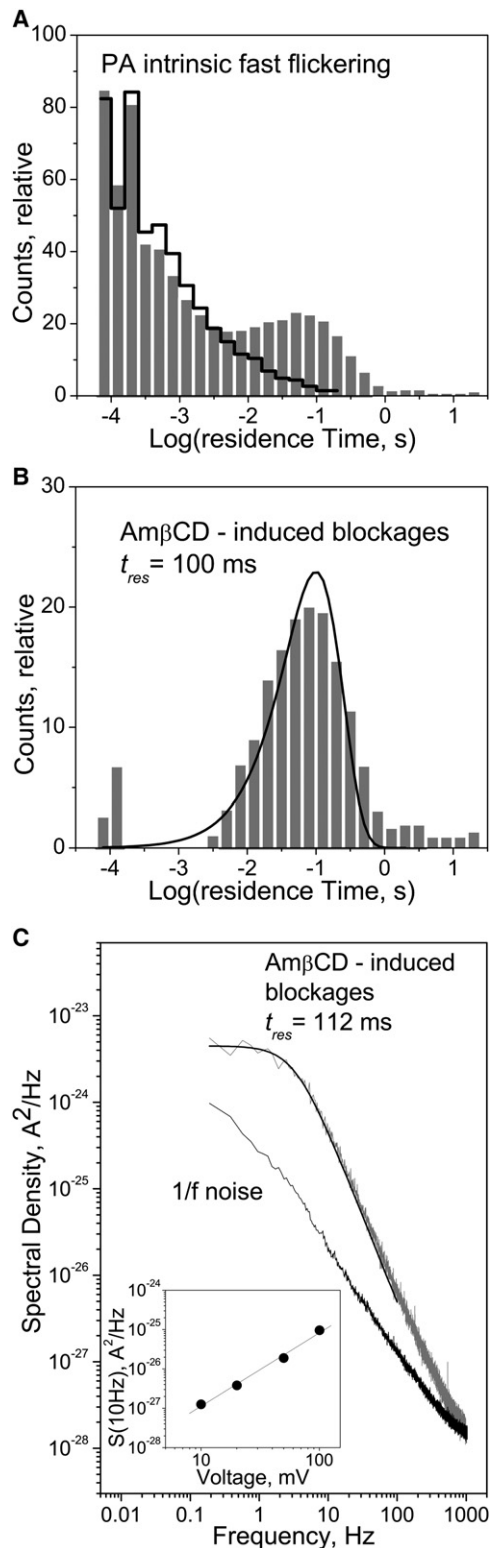


FIGURE 4 Analysis of single-channel flickering and blocking events. (A) Typical time histograms of PA₆₃ current fluctuations. (Solid histogram) Time-resolved events of fast flickering taken in AmPrβCD-free solution. (Shaded columns) Time-resolved events recorded in the presence of the blocker that include both the fast flickering and AmPrβCD-induced blockages. Currents recordings were filtered with 1500 Hz. (B) The histogram was obtained as the difference between the shaded and solid histograms

concentrations and higher voltages, time-histograms similar to the one shown in Fig. 4 B were obtained by directly measuring of the blockage times after current recordings had been filtered with a low-pass filter. This allowed us to get rid of the most of fast-flickering gating events (see also Fig. 3B in (7) or Fig. 11B in (8)).

To additionally validate the results of our time distribution analysis, we also analyzed the power spectrum density of current fluctuations. Results for the AmPrβCD-induced noise shown in Fig. 4 C (shaded line) demonstrate a good fit by a Lorentzian power spectrum at $f < 100$ Hz (smooth solid line through the experimental curve). The lower spectrum represents PA₆₃ $1/f$ -like noise measured in AmPrβCD-free solution at the type II insertion. The inset shows that $1/f$ current noise scales as the voltage-squared, i.e.,

$$d\lg S(10 \text{ Hz})/d\lg V = 1.96 \pm 0.28.$$

This implies that the fast flickering of the channel conductance discussed above does not depend on the applied voltage. In the case of type I insertion, an additional high-frequency spectral component (data not shown) was also observed. This extra noise is clearly seen in Fig. 3 A (left) for the open state of the channel.

A single-Lorentzian shape of the power spectral density is usually associated with a two-state Markov process, where both the residence time in the blocked state and the channel lifetime in the unblocked state (the time between successive blockages) are described by exponential distributions. As this assertion was verified experimentally, we use the two-state Markovian model of the blockage in the further discussion. The average lifetime of the blocked state, which is presumably the residence time of AmPrβCD in the channel pore, can be found as $t_{\text{res}} = 1/(2\pi f_c(1-p))$, while the average time between the blockages is $t_{\text{open}} = 1/(2\pi f_c p)$, where f_c is the corner frequency of the Lorentzian and p is the probability of finding the channel in the blocked state (25). In an ideal case of a channel that is free from its own gating, the probability for the channel to be in the blocked state is

$$p^{(\text{no gating})} = (I_o - I_{\text{ave}})/I_o,$$

where I_o is the current through the fully open channel, and I_{ave} is the average current through the channel in the presence of the blocker. To correct the open channel current values for the fast flickering we assumed that the blockage and

from Fig. 4 A and fitted by direct single-exponential (i.e., log probability) fitting as described in Sigworth and Sine (37). The fits were obtained using variable metrics as a search method and maximum likelihood as a minimization method. (C) Power spectral densities of AmPrβCD-induced PA₆₃ current fluctuations (shaded spectrum) at frequencies < 100 Hz can be fitted by the single Lorentzian in contrast to $1/f$ -like noise in the absence of AmPrβCD (black spectrum). (Inset) Spectral densities of $1/f$ -like noise calculated as averages over the range of 9.8–10.2 Hz as a function of voltage. Other experiments were performed under 50-mV applied voltage. Shaded histogram and current spectrum were calculated for 13.2 nM AmPrβCD bulk concentration. PC membranes were bathed by 1 M KCl and 5 mM MES at pH 6.6.

fast flickering are statistically independent processes with well-separated characteristic timescales. This leads to the following equation for the probability of finding the channel in the blocked state

$$p = \frac{I_{\text{ave}}^{(\text{control})} - I_{\text{ave}}}{I_{\text{ave}}^{(\text{control})}}, \quad (1)$$

where $I_{\text{ave}}^{(\text{control})}$ is the average current through the same channel measured before AmPr β CD addition into the solution. As for the much longer channel closures due to the voltage gating discussed above, they were excluded before the open probability analysis.

The assumption of independence of the blockage and fast flickering proved to be reasonable. Note that the time histogram fitting (Fig. 4B) and noise analysis (Fig. 4C) gives quite close values for t_{res} , 100 ms and 112 ms, respectively. However, the deviations are more significant than were found in the case of ampicillin-induced blockages of OmpF (20). This is probably related to some unavoidable systematic errors due to the broad time distribution of the fast flickering process. The t_{res} values given in the graphs are the averages of the values obtained in the two approaches outlined above.

Fig. 3B shows that the residence times are independent of the AmPr β CD bulk concentration. This observation agrees well with the first-order kinetics assumed for dissociation of the blocker-channel complex. The average residence time was close to 110 ms under 50-mV applied voltage for both types of channel insertions (Fig. 3B). The average time between successive blockages, t_{open} , is inversely proportional to the blocker concentration in accordance with the bimolecular model of the process and is independent of the type of insertion.

Blockage without translocation

Fig. 5 shows kinetic parameters of AmPr β CD binding to the channel as functions of the applied transmembrane voltage. The stepwise transitions in Fig. 5A reflect the complete blockage of the channel presumably as a result of the reversible binding of the positively charged AmPr β CD to the negatively charged residues (16–18) inside the PA₆₃ pore lumen. Fig. 5B shows that the dependence of the residence time on the applied voltage is close to exponential and does not show any cross-over behavior characteristic for translocating blockers. On the contrary, the on-time, t_{open} , is practically voltage-independent (Fig. 5C). Here we use $k_{\text{on}} = 1/(t_{\text{open}}c_{\text{bloc}})$, where c_{bloc} is the blocker bulk concentration, instead of t_{open} that allows us to compare results obtained at different blocker concentrations.

We did not observe any influence of bathing solution pH on the kinetic parameters of AmPr β CD binding under the range of pH 4–6.6 used in this study (data not shown). This observation indicates that neither the positively charged amino groups carried by AmPr β CD molecule nor the amino-acid residues inside the channel involved in AmPr β CD binding change their ionization states in this pH interval.

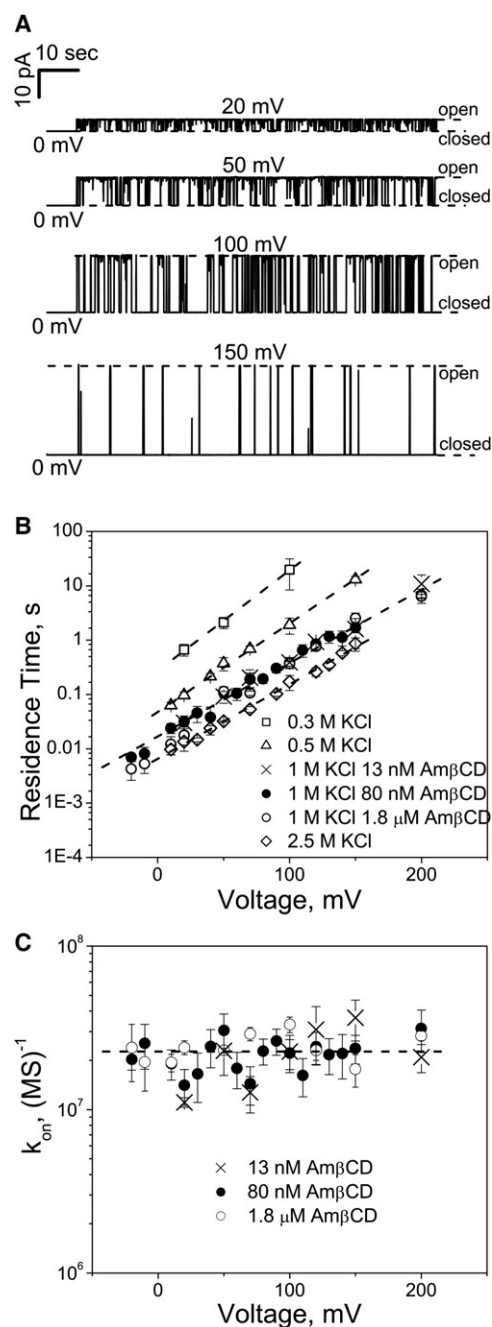


FIGURE 5 Kinetic parameters of AmPr β CD binding as functions of transmembrane voltage. (A) Typical current tracks in the presence of AmPr β CD show strong dependence on the applied voltage. Time averaging used for the plots was 50 ms. (B) The AmPr β CD residence time grows nearly exponentially with the transmembrane voltage. Data were obtained at 0.3 M (\square), 0.5 M (\triangle), 1 M (13 nM AmPr β CD, \times); 80 nM AmPr β CD, \bullet ; 1.8 μ M AmPr β CD, \circ), and 2.5 M KCl (\diamond) concentrations. The straight dashed lines represent linear fits through the data. (C) The on-rate constant, k_{on} , of AmPr β CD binding to the channel at 1 M KCl. (Dashed line) average value for all data points.

The crucial involvement of electrostatic interactions is suggested by the strong dependence of blockage parameters on the salt concentration shown in Fig. 6. High salt

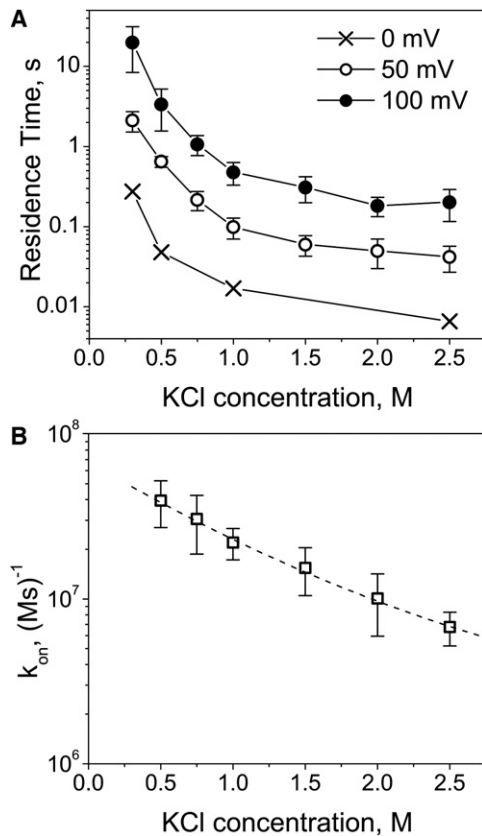


FIGURE 6 Kinetic parameters of AmPr β CD binding as functions of the KCl concentration in the bulk. Both the AmPr β CD residence time, t_{res} (A) and on-rate constant, k_{on} (B) decrease with the KCl concentration. The membranes were formed from PC. The bathing solution contained 5 mM MES at pH 6.6 and varied AmPr β CD concentration. The values of the residence times at zero voltage were obtained using the data shown in Fig. 5 B. AmPr β CD concentration varied from 3 nM to 1.5 μ M depending on KCl concentration.

concentrations are expected to reduce electrostatic forces significantly by screening out charges on both the blocker and the protein. This screening is most likely the cause of the two orders of magnitude decrease in the residence time plotted in Fig. 6 A. Fig. 6 B demonstrates that the on-rate constant, k_{on} , also decreases as the KCl bulk concentration increases. Since variation of the KCl concentration leads to significant changes in the on-rate of AmPr β CD binding, the results shown in Fig. 6 were obtained at different concentrations of the blocker, 3 nM to 1.5 μ M. This was necessary to collect reliable statistics.

Two modes of AmPr β CD action on the channel

Equilibrium dissociation constants at the single- and multichannel levels

From the single-channel data, we can find the equilibrium dissociation constant of the blocking reaction as

$$K_D^{(single)} = \frac{k_{off}}{k_{on}}, \quad (2)$$

where $k_{off} = 1/t_{res}$ and $k_{on} = 1/(t_{open}c_{bloc})$. Alternatively, using multichannel data, the dissociation constant can be found as

$$K_D^{(multi)} = \frac{(1-R)c_{bloc}}{R}, \quad (3)$$

where R is the relative reduction of current through a multichannel system due to the inhibitor addition. In many practical cases researchers use the so-called 50% inhibitory concentration, IC_{50} , which is given by Eq. 3 at $R = 0.5$. This parameter was used to analyze the multichannel experiments reported earlier (7,8). For the two-state model of blocking, the equilibrium dissociation constants calculated according to Eqs. 2 and 3 should be identical and independent of the blocker concentration. However, we found that this is not the case. Comparison of the K_D values obtained in our single- and multichannel measurements under otherwise identical conditions showed a statistically significant difference in all experiments whenever salt concentration in the membrane-bathing solution was below 1.5 M.

Fig. 7 A gives a typical example of a raw data titration curve in a multichannel experiment in 1 M KCl at 50 mV for PC bilayers. The conductance was measured for each consecutive AmPr β CD addition after the current had stabilized. The 50% inhibitory concentration is $IC_{50} = (1.8 \pm 0.9) \times 10^{-7}$ M. This value is one order of magnitude lower than the dissociation constant measured in single-channel experiments, $K_D^{(single)} = (1.2 \pm 0.5) \times 10^{-6}$ M.

We compared multichannel IC_{50} , and single-channel $K_D^{(single)}$ values at different bathing electrolyte concentrations (Fig. 7 B). Open circles represent dissociation constants calculated using Eq. 2 directly from kinetic parameters for single-channel measurements given in Fig. 5 whereas stars represent the IC_{50} values obtained in the corresponding multichannel experiments (7). Although $K_D^{(single)}$ and IC_{50} coincide at 1.5 M and higher KCl concentrations, at lower salt concentrations IC_{50} can be significantly smaller than $K_D^{(single)}$. The blocker appears to be more effective at the multichannel level. This discrepancy can be explained by the observation that AmPr β CD not only caused the reversible blockages described above but also significantly enhanced PA₆₃ voltage gating, especially at small KCl concentrations.

To quantify this observation, we determined single-channel $K_D^{(single)}$ values using 1-h-long current recordings that included prolonged closures due to voltage gating (*solid squares* in Fig. 7 B). All probability values were obtained by using Eq. 1, which now took into account possible voltage gating as well as the fast flickering contribution. Fig. 7 B shows that this correction essentially merges single-channel $K_D^{(single)}$ data with the corresponding multichannel IC_{50} values.

In addition, we found that at low salt concentrations, AmPr β CD's ability to promote gating is lipid-dependent.

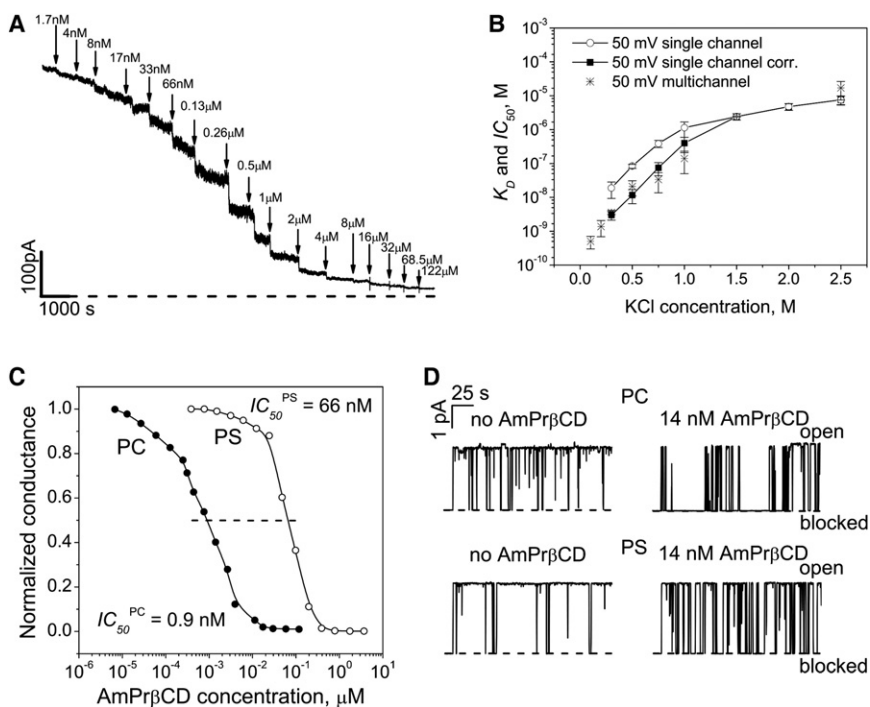


FIGURE 7 AmPr β CD pore inhibition compared at multi- and single-channel levels. (A) Multi-channel conductance as a function of AmPr β CD concentration. The current recording was filtered by averaging over 1 s intervals. (B) K_D and IC_{50} values of channel-blocker interaction increase with KCl bulk concentration in both single- (open circles) and multi-channel experiments (stars). (Solid squares) Single-channel data corrected for the AmPr β CD-induced voltage gating (see text). (C) Typical multi-channel titration curves for channels in PC (solid circles) and PS (open circles) membranes. The AmPr β CD 50% inhibitory concentration depends on the lipid membrane composition, giving IC_{50} as 0.9 nM and 66 nM for PC and PS, respectively. The applied voltage was 20 mV; membrane bathing solution was 0.1 M KCl at pH 6.6. (D) 14 nM AmPr β CD addition modifies ion currents for both PC (top) and PS (bottom) membranes (50 mV, 0.3 M KCl) but the probability to find the channel in the prolonged closed state is significantly higher for PC. Time averaging used for the plots was 500 ms.

Similarly to the voltage-induced effect in the absence of the blocker (Fig. 2 C), it is significantly weaker for the negatively charged (PS) membranes than for the neutral (PC) ones. Fig. 7 C gives two examples of the typical multi-channel titration curves obtained in PC (solid circles) and PS (open circles) membranes in 0.1 M KCl at 20 mV of the applied voltage. Comparison shows that PA $_{63}$ channels in the negatively charged lipid are \sim 70 times less sensitive to AmPr β CD inhibition. This difference virtually disappears at high KCl concentrations (data not shown). Fig. 7 D compares short fragments of single-channel currents recordings in PC and PS without AmPr β CD and in the presence of 14 nM AmPr β CD at 0.3 M KCl concentration. Control experiments (left) show that at 50 mV the gating is slightly more pronounced in PC membranes. In the case of PS membranes (Fig. 7 D, bottom), AmPr β CD presence in the *cis* bathing solution causes intense reversible blockages with $t_{res} = (1.8 \pm 0.6)$ s but does not significantly modify voltage gating. In contrast, for the channel in the PC membrane in addition to blockages with $t_{res} = (2.1 \pm 0.5)$ s, significant gating enhancement is seen (Fig. 7 D, top)). $K_D^{(single)}$ values calculated with the probability of the open state corrected as described above were equal to 2.4×10^{-8} M and 1.1×10^{-9} M for PS and PC membranes correspondingly. As seen from Fig. 7 B, these values are in agreement with IC_{50} values obtained from multichannel experiments.

Cis versus trans AmPr β CD addition

In the experiments described above we studied PA $_{63}$ channel behavior under conditions in which the blocker was added only to the *cis* side of the membrane. As is well-known

(5,11–14,21), insertion of PA $_{63}$ is always directional, and the *cis* side application of the blocker is physiologically relevant. In view of the channel asymmetry, we also performed a series of experiments adding the compound to the *trans* side of the membrane (data not shown). We found that this brings the channel to a low-conductance substate, i.e., the blockage is incomplete. In contrast to the *cis* addition, the effect is irreversible within the time limits of our experiment. Even at 3 M KCl solutions, the *trans* AmPr β CD binding could not be reversed. We also performed multichannel experiments to compare the effects of the *cis* and *trans* additions of the blocker. It turned out that the titration curve at *trans* AmPr β CD addition is more expanded and becomes saturated at \sim 25% of the original current, which corresponds to the residual conductance of the low-conductance substate. Therefore, even though AmPr β CD blocks the pore from either side, its action is qualitatively different as is witnessed by both single-channel and multichannel experiments.

Physiological relevance of AmPr β CD-PA $_{63}$ interaction

In our previous study, we reported a reasonably good correlation between the IC_{50} data for a number of cationic β -cyclodextrin derivatives obtained from cytotoxicity inhibitions and from multichannel lipid membrane experiments (Fig. 13 in (8)), whereas neutral and negatively charged cyclodextrins turned out to be inefficient (7). The most active of the tested compounds (No. 14B, Table I in (8)) was also reported to be the most efficient not only in protecting the cells against the anthrax toxicity but also in animal studies (9). The physicochemical aspects of the AmPr β CD - PA $_{63}$

interaction revealed by this study further support our idea that AmPr β CD inhibits anthrax toxins by means of electrostatic blockage of the PA₆₃ channels. Though we do not know at what stage of the anthrax toxin's cell journey β -cyclodextrins bind to PA, lipid bilayer experiments strongly suggest that the inhibitor binds to the PA₆₃ channel. It is believed that the channel formation takes place in the acidic environments of the endosomes only. On the other hand, fluorescent microscopy data (26) indicate that β CD might also bind to the PA₆₃ precursor – the receptor-bound heptameric prepore – before endocytosis takes place.

Regardless of the stage of the initial binding, conditions of our experiments may mimic those existing in vivo. First, we find that AmPr β CD blocks the channel from the physiologically relevant extracellular (or endosomal) side of the membrane. Second, the sign of the voltage gradient in an acidified endosome membrane was reported to be inside positive ($\varphi^{\text{endosome}} > \varphi^{\text{cytosol}}$) with $\Delta\varphi$ close to $+(10 - 30)$ mV ((27–29), see also discussion in (6)). The direction of this voltage gradient and its magnitude are within the range we use in the measurements.

At low salt concentrations, we find that the AmPr β CD's ability to promote channel closure is lipid-dependent. At this point, however, it is not clear if the second type of AmPr β CD action – the enhancement of voltage gating – has any significance in vivo since the nature of this phenomenon is not yet understood. In addition, the endosome's lipid composition and the ratio of neutral to negatively charged lipids endure significant changes during the endocytic pathway from the early endosomes to the late endosomes (30). It is not known at what stage of endocytic route LF and EF factors exit the endosome to intoxicate the cell (31). Therefore, it is not clear what lipid composition should be considered as physiologically relevant.

CONCLUDING REMARKS

In conclusion, major results of this work are as follows:

1. The AmPr β CD residence time exponentially increases with the applied voltage positive from the side of the blocker addition (*cis* side of the membrane) within the whole range of the voltages up to +200 mV and does not show the crossover behavior observed in experiments with tetraalkylammonium and chloroquine blockage (11–14). This implies that AmPr β CD does not go through the channel. Additional support for this inference is provided by the fact that blocking is quite different when the blocker is added to the *trans* side of the membrane.
2. The on-rate of the channel blockage by AmPr β CD does not depend on the applied voltage.
3. Both the on-rate and off-rate are influenced by the salt concentration in the bulk, giving much stronger off-rate salt dependence than that in the case of chloroquine blockage (14).

4. At salt concentrations smaller than 1.5 M, the inhibitive action of AmPr β CD is bimodal, in the sense that the reversible blockage described by a two-state Markov process acts in parallel with the AmPr β CD-enhanced voltage gating.
5. Most importantly, the 50% inhibitory concentration of AmPr β CD is orders-of-magnitude smaller than that of mono- and doubly-charged compounds (11–15), thus making per-substituted positively charged derivatives of β -cyclodextrin the most potent small-molecule inhibitors of the PA₆₃ channel that are found to date.

Blockage of channels by small-molecule charged compounds was addressed in a great number of studies. The most popular approach to the problem is based on the classical Woodhull model (32) and its multiple modifications that allow for more complex structures and for blocker-ion interactions. The model usually assumes the existence of two barriers and a well in-between, representing the localized binding site, whose positions in the channel determine the voltage dependence of the blockage. Such a model was used by Blaustein et al. (11–13) to interpret the blockage of PA₆₃ channel by single-charged tetraalkylammonium derivatives. According to Orlik et al. (14), this model also provided a good description of the channel blockage by chloroquine and related double-charged compounds.

The question arises whether the site model of PA₆₃ channel blockage suggested by Blaustein et al. (11–13) is applicable to the blockage by AmPr β CD. The point is that the diameter of β -cyclodextrin used as the initial scaffold for AmPr β CD synthesis is ~ 15 Å (Fig. 1), while the diameter of the channel *cis* side entrance according to tetraalkylammonium sizing (11–13) is only 12 Å. Therefore, the AmPr β CD derivative cannot reach the same blockage site as tetraalkylammonium derivatives, but the off-rate is nevertheless voltage dependent. Most probably, AmPr β CD binds in the channel vestibule area, and the voltage drop is not localized on the membrane. Earlier, assuming that AmPr β CD carries a charge of +7, we estimated the “electrical distance” to the blockage site to be close to 15% of the total channel length (7). We believe that a model based on continuum dynamics of the blocker in the channel vestibule could be more appropriate for the description of the blockage process. Corresponding theory will be developed in a forthcoming publication in the framework of the diffusive model of the particle motion in a membrane channel (33).

Authors are grateful to Adrian Parsegian, Kamran Melikov, and Roland Benz for helpful discussions.

This study was supported by the Intramural Research Program of the National Institutes of Health, the Center for Information Technology, and the Eunice Kennedy Shriver National Institute of Child Health and Human Development, and the National Institute of Allergy and Infectious Diseases (NIAID) Intramural Biodefense Research grant for institutes other than NIAID. V.A.K. is an employee and shareholder of Innovative Biologics, Inc.

REFERENCES

- Collier, R. J. 2009. Membrane translocation by anthrax toxin. *Mol. Aspects Med.* 30:413–422.
- Moayeri, M., and S. H. Leppla. 2009. Cellular and systemic effects of anthrax lethal toxin and edema toxin. *Mol. Aspects Med.* 30:439–455.
- Petosa, C., R. J. Collier, ..., R. C. Liddington. 1997. Crystal structure of the anthrax toxin protective antigen. *Nature.* 385:833–838.
- Katayama, H., B. E. Janowiak, ..., M. T. Fisher. 2008. GroEL as a molecular scaffold for structural analysis of the anthrax toxin pore. *Nat. Struct. Mol. Biol.* 15:754–760.
- Blaustein, R. O., T. M. Koehler, ..., A. Finkelstein. 1989. Anthrax toxin: channel-forming activity of protective antigen in planar phospholipid bilayers. *Proc. Natl. Acad. Sci. USA.* 86:2209–2213.
- Krantz, B. A., A. Finkelstein, and R. J. Collier. 2006. Protein translocation through the anthrax toxin transmembrane pore is driven by a proton gradient. *J. Mol. Biol.* 355:968–979.
- Karginov, V. A., E. M. Nestorovich, ..., S. M. Bezrukov. 2005. Blocking anthrax lethal toxin at the protective antigen channel by using structure-inspired drug design. *Proc. Natl. Acad. Sci. USA.* 102:15075–15080.
- Karginov, V. A., E. M. Nestorovich, ..., S. M. Bezrukov. 2006. Search for cyclodextrin-based inhibitors of anthrax toxins: synthesis, structural features, and relative activities. *Antimicrob. Agents Chemother.* 50:3740–3753.
- Moayeri, M., T. M. Robinson, ..., V. A. Karginov. 2008. In vivo efficacy of β -cyclodextrin derivatives against anthrax lethal toxin. *Antimicrob. Agents Chemother.* 52:2239–2241.
- Gu, L. Q., O. Braha, ..., H. Bayley. 1999. Stochastic sensing of organic analytes by a pore-forming protein containing a molecular adapter. *Nature.* 398:686–690.
- Blaustein, R. O., and A. Finkelstein. 1990. Voltage-dependent block of anthrax toxin channels in planar phospholipid bilayer membranes by symmetric tetraalkylammonium ions. Effects on macroscopic conductance. *J. Gen. Physiol.* 96:905–919.
- Blaustein, R. O., E. J. A. Lea, and A. Finkelstein. 1990. Voltage-dependent block of anthrax toxin channels in planar phospholipid bilayer membranes by symmetric tetraalkylammonium ions. Single-channel analysis. *J. Gen. Physiol.* 96:921–942.
- Blaustein, R. O., and A. Finkelstein. 1990. Diffusion limitation in the block by symmetric tetraalkylammonium ions of anthrax toxin channels in planar phospholipid bilayer membranes. *J. Gen. Physiol.* 96:943–957.
- Orlik, F., B. Schiffer, and R. Benz. 2005. Anthrax toxin protective antigen: inhibition of channel function by chloroquine and related compounds and study of binding kinetics using the current noise analysis. *Biophys. J.* 88:1715–1724.
- Krantz, B. A., R. A. Melnyk, ..., R. J. Collier. 2005. A phenylalanine clamp catalyzes protein translocation through the anthrax toxin pore. *Science.* 309:777–781.
- Benson, E. L., P. D. Huynh, ..., R. J. Collier. 1998. Identification of residues lining the anthrax protective antigen channel. *Biochemistry.* 37:3941–3948.
- Aguilella-Arzo, M., J. Cervera, ..., S. Mafé. 2006. Blocking of an ion channel by a highly charged drug: modeling the effects of applied voltage, electrolyte concentration, and drug concentration. *Phys. Rev. E.* 73:041914–1–6.
- Nguyen, T. L. 2004. Three-dimensional model of the pore form of anthrax protective antigen. Structure and biological implications. *J. Biomol. Struct. Dyn.* 22:253–265.
- Montal, M., and P. Mueller. 1972. Formation of bimolecular membranes from lipid monolayers and a study of their electrical properties. *Proc. Natl. Acad. Sci. USA.* 69:3561–3566.
- Nestorovich, E. M., C. Danelon, ..., S. M. Bezrukov. 2002. Designed to penetrate: time-resolved interaction of single antibiotic molecules with bacterial pores. *Proc. Natl. Acad. Sci. USA.* 99:9789–9794.
- Shenoy, D. K., W. R. Barger, ..., J. J. Kasianowicz. 2005. Functional reconstitution of protein ion channels into planar polymerizable phospholipid membranes. *Nano Lett.* 5:1181–1185.
- Kintzer, A. F., K. L. Thoren, ..., B. A. Krantz. 2009. The protective antigen component of anthrax toxin forms functional octameric complexes. *J. Mol. Biol.* 392:614–629.
- Anderson, D. S., and R. O. Blaustein. 2008. Preventing voltage-dependent gating of anthrax toxin channels using engineered disulfides. *J. Gen. Physiol.* 132:351–360.
- Delcour, A. H. 2002. Structure and function of pore-forming β -barrels from bacteria. *J. Mol. Microbiol. Biotechnol.* 4:1–10.
- Kullman, L., M. Winterhalter, and S. M. Bezrukov. 2002. Transport of maltodextrins through maltoporin: a single-channel study. *Biophys. J.* 82:803–812.
- Backer, M. V., V. Patel, ..., J. M. Backer. 2007. Inhibition of anthrax protective antigen outside and inside the cell. *Antimicrob. Agents Chemother.* 51:245–251.
- Van Dyke, R. W., and J. D. Belcher. 1994. Acidification of three types of liver endocytic vesicles: similarities and differences. *Am. J. Physiol.* 266:C81–C94.
- Rybak, S. L., F. Lanni, and R. F. Murphy. 1997. Theoretical considerations on the role of membrane potential in the regulation of endosomal pH. *Biophys. J.* 73:674–687.
- Sonawane, N. D., J. R. Thiagarajah, and A. S. Verkman. 2002. Chloride concentration in endosomes measured using a ratioable fluorescent Cl^- indicator: evidence for chloride accumulation during acidification. *J. Biol. Chem.* 277:5506–5513.
- van Meer, G., D. R. Voelker, and G. W. Feigenson. 2008. Membrane lipids: where they are and how they behave. *Nat. Rev. Mol. Cell Biol.* 9:112–124.
- Puhar, A., and C. Montecucco. 2007. Where and how do anthrax toxins exit endosomes to intoxicate host cells? *Trends Microbiol.* 15:477–482.
- Woodhull, A. M. 1973. Ionic blockage of sodium channels in nerve. *J. Gen. Physiol.* 61:687–708.
- Bezrukov, S. M., A. M. Berezhkovskii, and A. Szabo. 2007. Diffusion model of solute dynamics in a membrane channel: mapping onto the two-site model and optimizing the flux. *J. Chem. Phys.* 127:115101.
- Lacy, D. B., H. C. Lin, ..., R. J. Collier. 2001. A model of anthrax toxin lethal factor bound to protective antigen. *Nature.* 414:229–233.
- Drum, C. L., S.-Z. Yan, ..., W. J. Tang. 2002. Structural basis for the activation of anthrax adenyl cyclase exotoxin by calmodulin. *Nature.* 415:396–402.
- Pannifer, A. D., T. Y. Wong, ..., R. C. Liddington. 2001. Crystal structure of the anthrax lethal factor. *Nature.* 414:229–233.
- Sigworth, F. J., and S. M. Sine. 1987. Data transformations for improved display and fitting of single-channel dwell time histograms. *Biophys. J.* 52:1047–1054.